Article

Not peer-reviewed version

Population-Level Assessment of Circumferential Flank Waviness Variability Using a ΔW1 Indicator Derived from CMM Measurements

Krisztián Horváth *

Posted Date: 27 February 2026

doi: 10.20944/preprints202602.1811.v1

Keywords: flank waviness; tooth-to-tooth variability; long-wavelength geometry; coordinate measuring machine (CMM); harmonic lobe analysis; gear manufacturing quality; ΔW1 indicator

 doi:10.20944/preprints202602.1811.v1

Article

Population-Level Assessment of Circumferential Flank Waviness Variability Using a ΔW1 Indicator Derived from CMM Measurements

Krisztián Horváth

Department of Whole Vehicle Engineering, Széchenyi István University, H-9026, Győr, Egyetem tér 1; horvath.krisztian@ga.sze.com; Tel.: +36203154841

Abstract

Long-wavelength flank waviness plays a critical role in the excitation behavior of geared transmissions. While coordinate measuring machine (CMM) exports provide detailed geometric information, conventional evaluations typically focus on individual tooth curves and do not quantify circumferential inhomogeneity across teeth. This study introduces a tooth-to-tooth long-wavelength waviness inhomogeneity indicator (ΔW1) derived directly from Klingelnberg-style MKA plot files and demonstrates its behavior on a large industrial dataset comprising 3375 measured gear parts. Each flank curve was detrended using a second-order polynomial fit, and lobe-based waviness amplitudes (W1–W3) were extracted via sine–cosine projection. The proposed ΔW1 metric was defined as the difference between the maximum and minimum W1 values across measured teeth within the same part. To eliminate measurement edge effects, a mid-section evaluation (10–90% of the face width) was additionally performed. Population-level analysis revealed consistent separation between geometrically homogeneous and inhomogeneous parts, with ΔW1 values in the most critical components exceeding 7–9 μm after mid-section filtering. Unsupervised clustering based on ΔW1 and maximum W1 further distinguished a defect-prone subset of parts exhibiting systematic long-wavelength modulation patterns. The results demonstrate that circumferential waviness variability can be quantified using standard CMM outputs without additional hardware or specialized measurement procedures. The proposed indicator provides a practical geometric screening tool for large production batches and establishes a reproducible framework for linking detailed flank geometry to manufacturing consistency assessment. Although acoustic validation is outside the scope of the present work, the metric is intended as an NVH-relevant geometric risk indicator for future vibroacoustic correlation studies.

Keywords: flank waviness; tooth-to-tooth variability; long-wavelength geometry; coordinate measuring machine (CMM); harmonic lobe analysis; gear manufacturing quality; ΔW1 indicator

1. Introduction

In modern geared transmissions, long-wavelength flank geometry is a decisive factor in load distribution, time-varying mesh stiffness (TVMS), and transmission error (TE), which are the primary excitation sources of gear vibration and noise. TE is widely recognized as the dominant source of gear whine and dynamic excitation [1], and it is directly influenced by manufacturing errors, misalignment, and flank deviations [2].

While micro-scale roughness mainly affects frictional behavior and lubrication conditions—as well as noise contributions related to sliding and tribological effects [3]—longer-wavelength deviations across the face width significantly modify contact patterns, load sharing, and mesh stiffness modulation [4]. Analytical and numerical studies confirm that tooth surface modifications and geometric deviations strongly affect TVMS and load transmission error (LTE), thereby altering dynamic tooth loads [5,6].

 doi:10.20944/preprints202602.1811.v1

Misalignment and flank form deviations further amplify TE and dynamic mesh forces, influencing both stiffness variation and excitation behavior [6,7]. Experimental investigations also demonstrate that excitation behavior is dominated more by flank modification and macro-geometry deviations than by fine-scale surface texture [8].

In industrial metrology practice, detailed flank and profile measurements are typically obtained using coordinate measuring machines (CMMs) and evaluated via tooth contact analysis (TCA) approaches to assess contact pattern evolution and TE functions [9]. However, evaluation procedures generally focus on individual tooth flanks and their compliance with micro- and macro-geometry specifications.

Although dynamic models clearly show that time-varying meshing parameters and geometric deviations alter frequency content and excitation harmonics [10], systematic quantification of circumferential tooth-to-tooth variability within a single gear is rarely addressed in a statistically consistent framework. Given that periodic flank modifications can intentionally shape excitation spectra [11], unintended circumferential variability may likewise introduce additional TE harmonics and dynamic mesh force components.

Overall, the literature consistently demonstrates that macro-geometry deviations and flank modifications significantly influence TE, mesh stiffness modulation, and dynamic excitation. Therefore, a systematic evaluation of circumferential variability between teeth could provide additional insight into manufacturing consistency and NVH-relevant excitation mechanisms.

Conventional waviness and flank form evaluation methods typically assess each measured curve independently, reporting parameters such as total profile deviation, lead slope, or harmonic components along the face width. This curve-based approach is consistent with established tooth contact analysis (TCA) and TE evaluation frameworks, which primarily focus on individual tooth geometry and its local meshing behavior [9].

Although these indicators adequately describe the geometric condition of a single tooth, they do not inherently capture circumferential tooth-to-tooth inhomogeneity within the same gear component. However, TE and dynamic excitation are known to be highly sensitive to geometric deviations, flank modifications, and misalignment effects [12]. Variations in flank geometry influence TVMS and dynamic tooth loads, thereby altering excitation spectra and vibration behavior [5].

In large production batches, circumferential variability between teeth may reflect process instability, tool wear progression, or localized machining effects. Experimental studies indicate that excitation behavior is dominated more by flank modification accuracy and macro-geometry deviations than by fine-scale surface texture [8], further emphasizing the relevance of long-wavelength geometric consistency.

Consequently, there is a justified need for a population-scale, geometry-based indicator capable of quantifying long-wavelength flank waviness variability across teeth using standard CMM outputs. Such an indicator would extend conventional single-curve evaluation toward a statistically consistent assessment of circumferential homogeneity, without requiring additional measurement hardware or dedicated NVH test benches.

To address this gap, the present study introduces a tooth-to-tooth long-wavelength waviness inhomogeneity indicator, denoted as $\Delta W1$. First, each measured flank curve is detrended using a second-order polynomial in order to remove global form components and isolate residual waviness. The first-order lobe amplitude (W1) is then extracted by projecting the residual signal onto sine and cosine basis functions along the normalized face width. For each gear component, $\Delta W1$ is defined as the difference between the maximum and minimum W1 values across the measured teeth on the same flank side. In this formulation, $\Delta W1$ represents the circumferential spread of long-wavelength waviness within a single part. To reduce the influence of measurement edge effects at the boundaries of the evaluation range, an additional mid-section calculation (10–90% of the face width) is performed, yielding a robust estimate of the intrinsic tooth-to-tooth variability.

 doi:10.20944/preprints202602.1811.v1

2. Materials and Methods

2.1. Measurement Data and File Structure

Figure 1. Processing workflow for long-wavelength flank waviness inhomogeneity assessment.

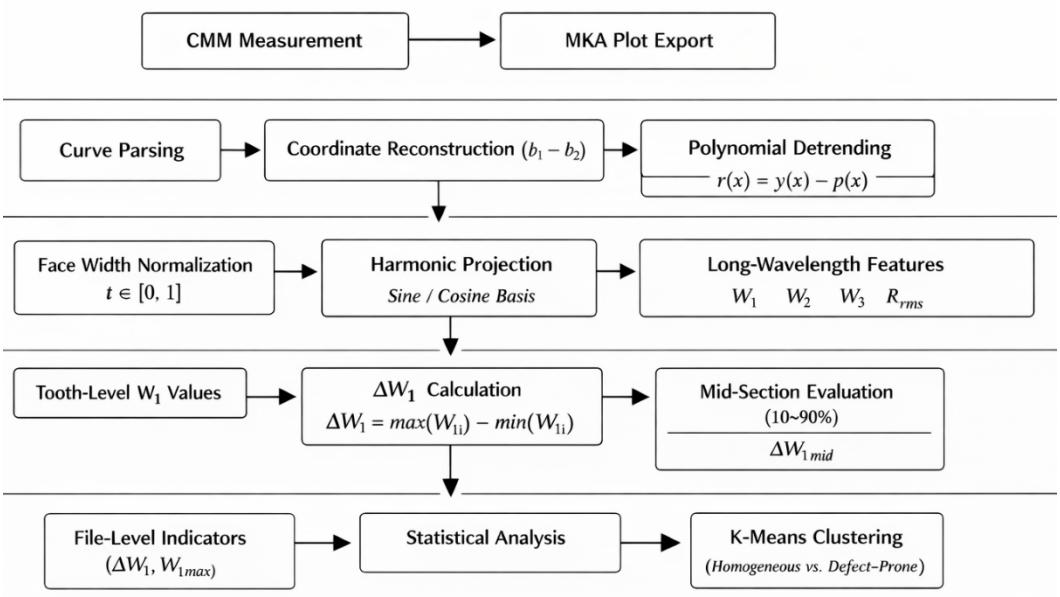

Figure 1. Processing workflow for long-wavelength flank waviness inhomogeneity assessment. Raw CMM MKA exports are parsed and detrended. Harmonic lobe amplitudes (W1–W3) are extracted via sine–cosine projection. The proposed ΔW1 indicator quantifies circumferential variability across teeth. Mid-section filtering suppresses edge effects. Population-level statistics and clustering enable identification of geometrically inconsistent components.

All components share the same macrogeometry. The investigated gears contain 23 teeth. Flank measurements were available on multiple teeth per component and at least one flank side, enabling tooth-to-tooth comparison within each part. The dataset represents serial production parts from multiple batches measured under a consistent CMM inspection routine.

The dataset consists of 3375 gear components measured using a coordinate measuring machine (CMM), with results exported in Klingelnberg-style MKA plot format. Each file contains flank and profile measurement blocks, including tooth identification, flank side (left/right), number of sampling points, and evaluation range parameters. Only flank measurements were considered for the present long-wavelength waviness analysis.

Each flank curve is represented by a sequence of sampled deviation values along the face width. The evaluation start and end positions are defined in the file header (b1. b2), enabling reconstruction of the physical coordinate axis. Undefined placeholder values are excluded prior to further processing.

2.2. Curve Detrending and Residual Signal Definition

To isolate waviness components from global form deviations, each flank curve was detrended using a second-order polynomial fit. Let y(x) denote the measured deviation along the face width coordinate x. A quadratic polynomial p(x) was fitted using least squares, and the residual signal was defined as:

$$r(x) = y(x) - p(x) \quad (1)$$

 doi:10.20944/preprints202602.1811.v1

The residual was subsequently mean-centered to remove constant offsets. This procedure suppresses global slope and curvature effects while preserving long-wavelength modulation patterns relevant to excitation behavior.

2.3. Long-Wavelength Lobe Feature Extraction (W1–W3)

Harmonic projection onto sine and cosine basis functions corresponds to the order-based spectral decomposition widely applied in TE and gear excitation analysis [13].

Long-wavelength waviness components were quantified using harmonic projection along the normalized face width. The coordinate was normalized to the unit interval:

$$t = \frac{x - x_{xmin}}{x_{xmax} - x_{xmin}}, \tag{2}$$

For each residual signal *r(t)*, harmonic amplitudes were computed via projection onto sine and cosine basis functions:

$$A_{k,sin} = \langle r(t), \sin(2\pi kt) \rangle \tag{3}$$

$$A_{k,cos} = \langle r(t), cos(2\pi kt) \rangle \tag{4}$$

The k-th lobe amplitude was then defined as:

$$W_k = 2\sqrt{A_{k,sin}^2 A_{k,cos}^2}, \tag{5}$$

In this study, the first three lobe components (W1–W3) were extracted. The first-order component (W1) represents the dominant long-wavelength modulation along the face width and forms the basis of the circumferential inhomogeneity indicator introduced below.

2.4. Definition of the Tooth-to-Tooth Inhomogeneity Indicator (ΔW1)

For each gear component and flank side, the tooth-to-tooth waviness inhomogeneity was quantified as:

$$\Delta W1 = \max(W1_i) - min(W1_i) \tag{6}$$

where $W1_i$denotes the first-order lobe amplitude of the i-th measured tooth on the same flank side.

This definition captures the circumferential spread of long-wavelength waviness within a single part. File-level aggregation was performed by taking the maximum ΔW1 value across measured sides. To mitigate potential edge-related measurement artifacts, an additional mid-section evaluation was conducted by restricting the analysis to the central 10–90% of the physical face-width coordinate range (based on reconstructed b1–b2 limits from the MKA header). The harmonic projection was fully recomputed on the truncated coordinate interval without interpolation or post-scaling, and ΔW1_mid was derived analogously from the recalculated W1 values.

2.5. Population-Level Analysis and Clustering

To explore structural grouping within the dataset, unsupervised K-means clustering was performed using two file-level features: ΔW1_max_side and the maximum tooth-level amplitude W1_max. Prior to clustering, both features were standardized to zero mean and unit variance to prevent scale dominance effects.

K-means clustering was applied following Lloyd's algorithm [14] with k-means++ initialization to improve convergence robustness [15]. The number of clusters was selected using the elbow criterion [16].

The number of clusters was set to k=3 based on inspection of the inertia curve using the elbow criterion, which is a commonly applied heuristic for cluster number selection in partition-based clustering [16]. K-means clustering was implemented according to Lloyd's algorithm [14] and

 doi:10.20944/preprints202602.1811.v1

initialized using the k-means++ strategy to improve centroid seeding robustness and convergence stability [15]. Multiple random initializations ($n_{init} = 10$) were performed to reduce sensitivity to local minima and enhance solution reliability.

This configuration enabled separation between a dominant low-variability cluster, an intermediate group, and a smaller high-variability subset characterized by elevated ΔW1 and W1_max values.

3. Results

3.1. Population-Level Distribution of W1 and ΔW1

The long-wavelength lobe amplitudes were evaluated across the complete measurement population. After excluding files with incomplete flank blocks, valid flank-based indicators were obtained for 3362 gear components, comprising 10,216 individual tooth-side curves. At tooth level, the first lobe amplitude W1 showed a median of 2.24 µm and a mean of 2.16 µm (95th percentile: 3.04 µm. 99th percentile: 3.41 µm). This indicates geometrically homogeneous long-wavelength flank modulation for most components in the investigated production batches.

Circumferential inhomogeneity was quantified using the proposed ΔW1 indicator, defined as the within-part tooth-to-tooth spread of W1. The file-level metric ΔW1_max_side exhibited a median of 0.41 µm and a mean of 0.72 µm, with the upper tail characterized by a 95th percentile of 2.37 µm and a maximum of 5.05 µm. The distribution therefore contains a distinct subset of parts with markedly higher tooth-to-tooth variability compared to the main population.

The statistical distribution of the extracted indicators is summarized in Table 1. While the majority of components exhibit low circumferential variability, the upper tail of the ΔW1 distribution indicates a limited subset of geometrically inconsistent parts.

Table 1. Statistical summary of long-wavelength waviness indicators across the evaluated gear population (N = 3362 valid parts).

Indicator	Mean (µm)	Median (µm)	95th Percentile (µm)	99th Percentile (µm)	Maximum (µm)
W1 (tooth-level)	2.16	2.24	3.04	3.41	~4.50
ΔW1_max_side	0.72	0.41	2.37	3.68	5.05

The population-level distribution of ΔW1_max_side is illustrated in Figure 2. The histogram reveals a strongly right-skewed distribution, with the majority of parts concentrated below 1 µm and a progressively thinning upper tail extending beyond 4 µm. This tail region corresponds to geometrically atypical components characterized by elevated circumferential waviness variability.

 doi:10.20944/preprints202602.1811.v1

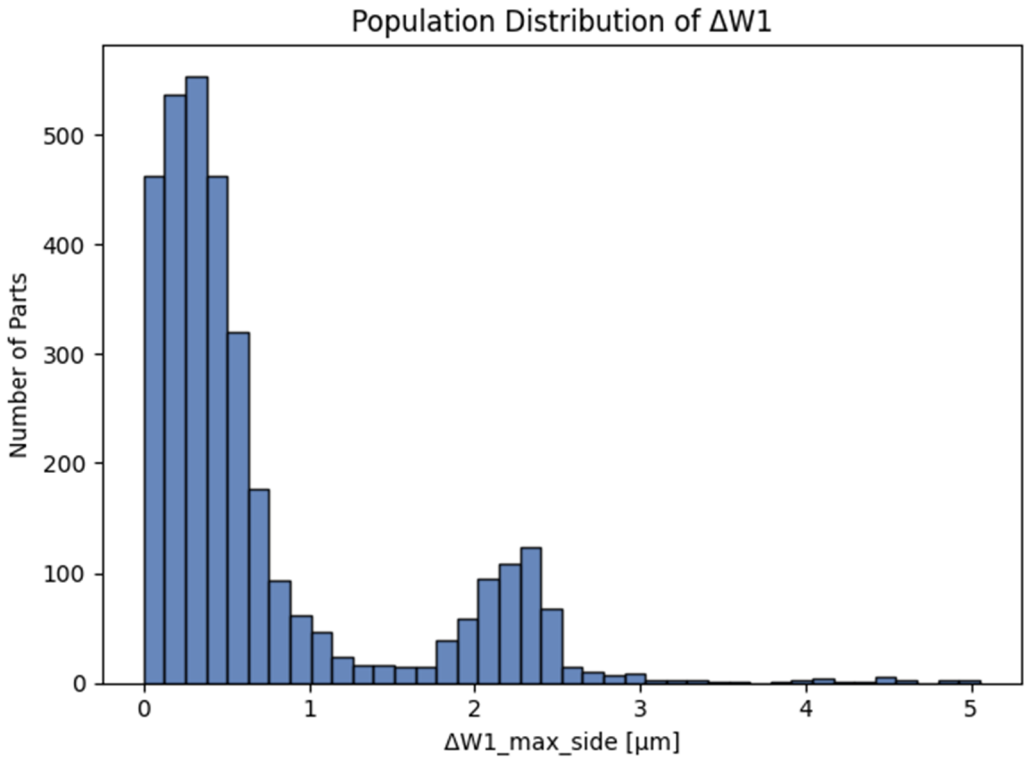

Figure 2. Population-level distribution of the circumferential inhomogeneity indicator ΔW1_max_side across the evaluated gear components. The majority of parts exhibit low tooth-to-tooth variability, while a distinct upper tail indicates a limited subset of geometrically inconsistent components. The 95th percentile threshold highlights the transition toward the defect-prone regime.

3.2. Effect of Mid-Section Evaluation (10–90% Face Width)

To assess robustness against boundary-related effects, an additional mid-section evaluation (10–90% of the face width) was applied. This filtering step increases sensitivity to intrinsic long-wavelength modulation by reducing edge-dominated deviations observed near the evaluation limits. While the full-population mid-section recomputation is not reported for all parts in the present manuscript due to space constraints, the recalculation procedure was applied consistently to all five critical components using the identical harmonic extraction workflow.

For the five most critical parts, mid-section recomputation yielded ΔW1_mid values in the range of approximately 7–9 µm, exceeding the corresponding full-length ΔW1 values. These values exceed the 99th percentile of the full-population ΔW1_max_side distribution by a factor of approximately two, indicating that the identified components represent statistical outliers within the dataset.

This confirms that the observed circumferential variability is not solely attributable to boundary artifacts and remains present within the central face-width region. These values refer exclusively to the five most critical components and do not represent the overall population distribution.

A direct comparison between full-length and mid-section recalculated values for the five most critical components is provided in Table 2. The systematic increase in ΔW1 after edge filtering confirms that circumferential inhomogeneity persists within the central face-width region. All mid-section values reported in Table 2 were independently recalculated using the truncated dataset and verified against the original full-length processing pipeline to exclude indexing or implementation inconsistencies.

 doi:10.20944/preprints202602.1811.v1

Table 2. Comparison of full-length and mid-section (10–90%) ΔW1 values for the five most critical components.

Part ID	W1_best_full (μm)	W1_worst_full (μm)	ΔW1_full (μm)	W1_best_mid (μm)	W1_worst_mid (μm)	ΔW1_mid (μm)
Part A	1.03	6.09	5.05	1.44	9.03	7.59
Part B	1.12	5.82	4.70	1.50	8.42	6.92
Part C	1.35	5.63	4.28	1.72	8.12	6.40
Part D	1.08	5.41	4.33	1.61	7.98	6.37
Part E	1.24	5.34	4.10	1.55	7.72	6.17

3.3. Identification of Defect-Prone Components

To explore structural grouping, K-means clustering was applied using two file-level features: **ΔW1_max_side** and the maximum tooth-level amplitude **W1_max**. With **k = 3**, the analysis separated a dominant low-variability cluster from intermediate and high-variability subsets. The smallest cluster contained **47 parts** and exhibited simultaneously elevated ΔW1 and W1_max, with cluster-center values of approximately **ΔW1 ≈ 3.68 μm** and **W1_max ≈ 5.70 μm**.

These results indicate that ΔW1, particularly when combined with W1_max, provides a practical geometry-based screening approach capable of isolating a defect-prone subset within large production batches.

A direct comparison between full-length and mid-section recalculated ΔW1 values for the five most critical components is presented in Figure 3. All points lie above the diagonal reference, indicating systematically increased inhomogeneity after boundary filtering. This behavior confirms that the identified variability is not dominated by edge artifacts but reflects intrinsic long-wavelength modulation differences.

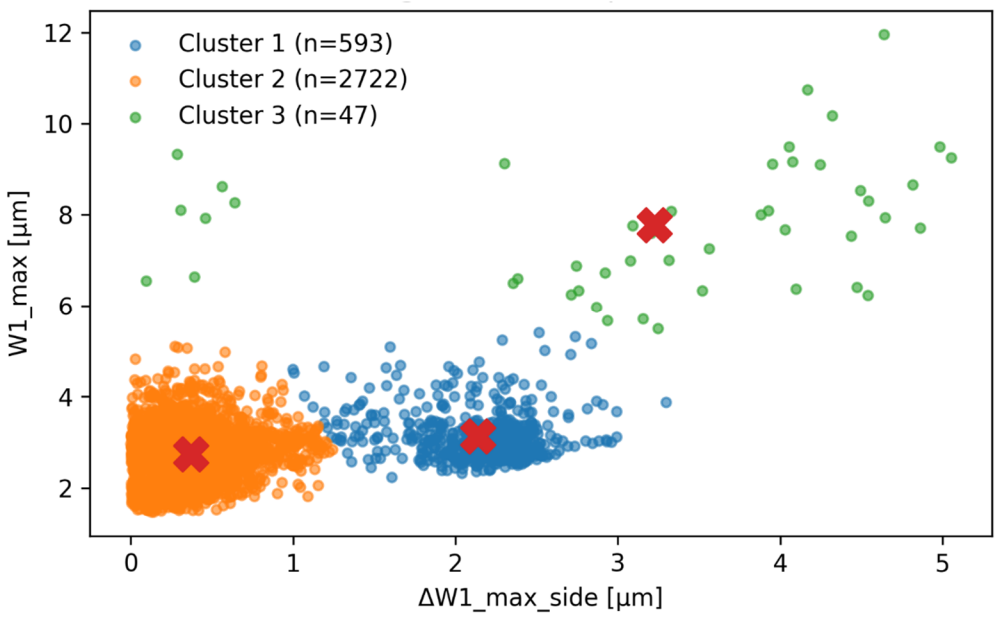

Figure 3. Comparison between full-length and mid-section (10–90%) ΔW1 values for the five most critical components. The diagonal reference line represents equality. All highlighted components exhibit increased ΔW1 after boundary filtering, confirming that circumferential inhomogeneity persists within the central face-width region.

 doi:10.20944/preprints202602.1811.v1

4. Discussion

The present study introduces ΔW1 as a geometry-based indicator for circumferential long-wavelength waviness inhomogeneity and evaluates its behavior across a large industrial dataset. Several aspects merit further interpretation.

First, the results confirm that conventional tooth-by-tooth evaluation is insufficient for detecting circumferential inconsistency within a gear component. Individual W1 values alone describe the long-wavelength modulation of a single flank curve but do not reveal whether modulation amplitudes vary systematically between teeth. The ΔW1 formulation explicitly captures this spread and therefore provides additional structural information about the part as a whole.

Second, the population-level analysis indicates that most components exhibit low ΔW1 values, suggesting stable manufacturing conditions in the majority of cases. The presence of a distinct upper tail in the distribution, however, points to a subset of parts with pronounced circumferential variability. Such variability may arise from tool wear, localized machining instabilities, clamping effects, or thermal drift during manufacturing. While the present work does not directly investigate process causality, the statistical separation observed in the dataset supports the interpretation of ΔW1 as a manufacturing consistency indicator.

Third, the mid-section evaluation demonstrates that boundary-related artifacts can influence full-length waviness amplitudes. The systematic increase in W1 after restricting the evaluation to the central 10–90% region suggests that edge regions may partially attenuate harmonic components. Importantly, the relative ranking of components remained stable, indicating that ΔW1 reflects intrinsic geometric variability rather than measurement artifacts alone.

From an NVH perspective, long-wavelength flank modulation can contribute to contact stiffness variation and TE excitation, particularly under load. However, the present study intentionally limits its scope to geometry-based assessment. No direct correlation with roll testing or End-of-Line acoustic measurements is included. Therefore, ΔW1 should not be interpreted as a validated acoustic predictor but rather as a geometric risk indicator potentially relevant for dynamic excitation studies.

Finally, the clustering results demonstrate that combining ΔW1 with maximum W1 amplitude enables automated screening of large production batches. The approach remains computationally lightweight and operates directly on standard CMM exports. This makes it compatible with existing quality control workflows without requiring additional hardware or measurement procedures.

5. Conclusions

This study introduced a tooth-to-tooth long-wavelength waviness inhomogeneity indicator (ΔW1) derived from standard CMM MKA plot exports and evaluated its behavior on a population of 3375 gear components. By combining second-order detrending, harmonic lobe extraction, circumferential aggregation, and mid-section robustness filtering, the proposed framework enables systematic quantification of flank waviness variability across teeth within a single part.

The results demonstrate that most components exhibit low circumferential variability, indicating stable geometric behavior at production scale. However, a distinct subset of parts shows elevated ΔW1 values, reflecting pronounced long-wavelength modulation differences between teeth. The mid-section evaluation confirmed that these differences are not solely driven by boundary effects but represent intrinsic geometric inhomogeneity.

Unsupervised clustering based on ΔW1 and maximum W1 amplitude further enabled automated separation between geometrically homogeneous and defect-prone components. The approach is computationally lightweight, requires no additional measurement hardware, and can be integrated into existing CMM-based quality assessment workflows.

Although no direct vibroacoustic validation is included in the present work, the proposed ΔW1 metric establishes a reproducible and scalable geometry-based screening indicator that may support future investigations linking flank waviness variability to dynamic excitation and NVH behavior.

Supplementary Materials: Supplementary materials include the aggregated feature dataset used for statistical analysis and clustering, provided in CSV format.

Funding: This research was supported by the EKÖP-25-3-I-SZE-82 University Research Scholarship Program of the Ministry for Culture and Innovation from the source of the National Research, Development and Innovation Fund.

Data Availability Statement: The processed feature-level dataset generated and analyzed during the current study is publicly available at Zenodo, DOI:: 10.5281/zenodo.18757468. Raw CMM MKA measurement files originate from industrial production and are not publicly available due to confidentiality restrictions.

Conflicts of Interest: The authors declare no conflicts of interest.

References

1. Sun, M., Lu, C., Liu, Z., Sun, Y., Chen, H., & Shen, C. (2020). Classifying, predicting, and reducing strategies of the mesh excitations of gear whine noise: A survey. Shock and Vibration, 2020, Article 9834939. https://doi.org/10.1155/2020/9834939
2. Radu, M., Andrei, L., & Andrei, G. (2018). A perspective on gear meshing quality based on transmission error analysis. IOP Conference Series: Materials Science and Engineering, 444, 052011. https://doi.org/10.1088/1757-899X/444/5/052011
3. Baumann, A., & Bertsche, B. (2022). Coefficient of friction behavior of gear oils and significance for the meshing process of spur gears. Forschung im Ingenieurwesen, 86, 795–805. https://doi.org/10.1007/s10010-022-00589-9
4. Kamycki, W., & Noga, S. (2020). Application of the thin slice model for determination of face load distribution along the line of contact and the relative load distribution measured along gear root. Strojniški Vestnik – Journal of Mechanical Engineering, 66(5–6), 300–310. https://doi.org/10.5545/sv-jme.2020.6555
5. Li, J., Zhao, H., Ren, Y., & Yang, J. (2025). Calculation of time-varying mesh stiffness of internal mesh transmission and analysis of influencing factors. Applied Sciences, 15, 4599. https://doi.org/10.3390/app15094599
6. Zhou, J., Yi, F., Xu, X., Lai, J., Liu, Y., & Dong, P. (2019). Effect of tooth profile modification on dynamic tooth load of planetary gear train. Shock and Vibration, 2019, Article 8156971. https://doi.org/10.1155/2019/8156971
7. Han, G., Yuan, B., & Qiao, G. (2021). Tooth surface modification for helical gear pairs considering mesh misalignment tolerance. Shock and Vibration, 2021, Article 5563648. https://doi.org/10.1155/2021/5563648
8. Trübswetter, M., Götz, J., Kohn, B., Otto, M., & Stahl, K. (2021). Effects of different hard finishing processes on gear excitation. Machines, 9(8), 169. https://doi.org/10.3390/machines9080169
9. Radu, M., Andrei, L., & Andrei, G. (2019). A survey on gear meshing quality based on tooth contact analysis. IOP Conference Series: Materials Science and Engineering, 514, 012027. https://doi.org/10.1088/1757-899X/514/1/012027
10. Song, J., Hou, L., Ma, R., Li, Z., Lin, R., Chen, Y., Chen, Y., & Saeed, N. (2025). Nonlinear dynamic modeling of a gear-bearing transmission system based on dynamic meshing parameters. Machines, 13(3), 230. https://doi.org/10.3390/machines13030230
11. Sepp, S., Wenig, A., Otto, M., & Stahl, K. (2023). Acoustical behavior of periodic flank modifications under dynamic operating conditions. Forschung im Ingenieurwesen, 87, 913–922. https://doi.org/10.1007/s10010-023-00685-4
12. Bai, B., Kuang, Y., Guo, W., & Mao, S. (2022). Influence of misalignment on beveloid gear tooth contact and dynamic characteristics in transfer case transmission of AWD vehicle. Shock and Vibration, 2022, Article 7565845. https://doi.org/10.1155/2022/7565845
13. Pedrero, J. I., Sánchez-Espiga, J., Sánchez, M. B., Pleguezuelos, M., Fernández-del-Rincón, A., & Viadero, F. (2024). Simulation and validation of the transmission error, meshing stiffness, and load sharing of planetary spur gear transmissions. Mechanism and Machine Theory. https://doi.org/10.1016/j.mechmachtheory.2024.105800

 doi:10.20944/preprints202602.1811.v1

14. Lloyd, S. P. (1982). Least squares quantization in PCM. IEEE Transactions on Information Theory, 28(2), 129–137. https://doi.org/10.1109/TIT.1982.1056489
15. Arthur, D., & Vassilvitskii, S. (2007). k-means++: The advantages of careful seeding. In Proceedings of the Eighteenth Annual ACM-SIAM Symposium on Discrete Algorithms (pp. 1027–1035). https://doi.org/10.1145/1283383.1283494
16. Jain, A. K. (2010). Data clustering: 50 years beyond K-means. Pattern Recognition Letters, 31(8), 651–666. https://doi.org/10.1016/j.patrec.2009.09.011